

Article

Wear Dry Behavior of the Al-6061-Al₂O₃ Composite Synthesized by Mechanical Alloying

Víctor Hugo Mercado-Lemus ^{1,*}, Cynthia Daisy Gomez-Esparza ², Juan Carlos Díaz-Guillén ¹, Jan Mayén-Chaires ³, Adriana Gallegos-Melgar ¹, Hugo Arcos-Gutierrez ³, Maricruz Hernández-Hernández ¹, Isaías Emmanuel Garduño ³, José Antonio Betancourt-Cantera ¹, and Raúl Perez-Bustamante ^{1,*}

¹ Cátedras Conacyt-Corporación Mexicana de Investigación en Materiales (COMIMSA), Ciencia y Tecnología No. 790, Fraccionamiento Saltillo 400, Saltillo CP 25290, Coahuila, Mexico; jcarlos@comimsa.com (J.C.D.-G.); adnagamel@gmail.com (A.G.-M.); maricruz.hernandez@ciateq.mx (M.H.-H.); jbetancourt@comimsa.com (J.A.B.-C.)

² Facultad de Ingeniería, Universidad Autónoma de Chihuahua, Chihuahua CP 31000, Chihuahua, Mexico; cynthiadaisy@gmail.com

³ Cátedras Conacyt-Centro de Tecnología Avanzada (CIATEQ), Zona Industrial del Potosí, San Luis Potosí CP 78395, San Luis Potosí, Mexico; jan.mayen@ciateq.mx (J.M.-C.); hugo.arcos@ciateq.mx (H.A.-G.); isaias.garduno@ciateq.mx (I.E.G.)

* Correspondence: vic_210583@yahoo.com.mx (V.H.M.-L.); raul.perez@comimsa.com (R.P.-B.); Tel.: +52-(444)-824-0310 (ext. 2760) (V.H.M.-L.)



Citation: Mercado-Lemus, V.H.; Gomez-Esparza, C.D.; Díaz-Guillén, J.C.; Mayén-Chaires, J.; Gallegos-Melgar, A.; Arcos-Gutierrez, H.; Hernández-Hernández, M.; Garduño, I.E.; Betancourt-Cantera, J.A.; Perez-Bustamante, R. Wear Dry Behavior of the Al-6061-Al₂O₃ Composite Synthesized by Mechanical Alloying. *Metals* **2021**, *11*, 1652. <https://doi.org/10.3390/met11101652>

Academic Editor:
Alexandre Emelyanenko

Received: 14 September 2021
Accepted: 14 October 2021
Published: 18 October 2021

Publisher's Note: MDPI stays neutral with regard to jurisdictional claims in published maps and institutional affiliations.



Copyright: © 2021 by the authors. Licensee MDPI, Basel, Switzerland. This article is an open access article distributed under the terms and conditions of the Creative Commons Attribution (CC BY) license (<https://creativecommons.org/licenses/by/4.0/>).

Abstract: The present research deals with the comparative wear behavior of a mechanically milled Al-6061 alloy and the same alloy reinforced with 5 wt.% of Al₂O₃ nanoparticles (Al-6061-Al₂O₃) under different dry sliding conditions. For this purpose, an aluminum-silicon-based material was synthesized by high-energy mechanical alloying, cold consolidated, and sintered under pressureless and vacuum conditions. The mechanical behavior was evaluated by sliding wear and microhardness tests. The structural characterization was carried out by X-ray diffraction and scanning electron microscopy. Results showed a clear wear resistance improvement in the aluminum matrix composite (Al-6061-Al₂O₃) in comparison with the Al-6061 alloy since nanoparticles act as a third hard body against wear. This behavior is attributed to the significant increment in hardness on the reinforced material, whose strengthening mechanisms mainly lie in a nanometric size and homogeneous dispersion of particles offering an effective load transfer from the matrix to the reinforcement. Discussion of the wear performance was in terms of a protective thin film oxide formation, where protective behavior decreases as a function of the sliding speed.

Keywords: aluminum matrix composites; alumina reinforcement; dry sliding conditions; ball-on-disk configuration

1. Introduction

The versatility of aluminum for different applications makes it an ideal structural material with high demand for aerospace, automotive, and other industries. Its mechanical properties are altered by adding alloying elements for the production or by incorporating reinforcing elements of different nature [1]. Being aluminum, one of the materials with the highest consumption globally by different industries, it represents an ideal material in manufacturing various components considered for structural applications. Secondary aluminum, obtained as waste material during the machining processes of such components [2], can be recycled by techniques requiring high energy consumption and, therefore, high cost. The reprocessing of metal shavings by mechanical means represents a low-cost alternative carried out at room temperature. Combined with techniques based on powder metallurgy and mechanical alloying, it represents a low energy consumption route in producing alloys and metal matrix composites.

The development of new materials is a subject of ongoing interest for the scientific community [3–5]. This recent attraction is due to the potential of micro- and nano-reinforcements to enhance the mechanical performance of the alloy [6]. Therefore, new materials synthesis aims to improve specific properties related to mechanical strength, ductility, corrosion resistance, and wear resistance.

Aluminum-based composite materials show interesting properties used in highly demanding engineering applications; however, their performance under load and wear conditions is crucial [1,4,5]. Consequently, the selection of the reinforcing material is a critical parameter in producing efficient composite materials. Therefore, the small size and homogeneous dispersion of ceramic particles provide composites a good combination of mechanical strength, hardness, and wear resistance [5]. Among them, alumina (Al_2O_3) particles have proven their efficiency in hardened ferrous alloys, high thermal stability, and non-formation of undesirable phases. On the other hand, their mechanical strength, hardness, high melting point, good thermal stability, and chemical inertia make them a material considered in non-ferrous alloys [7–12].

In this regard, several research groups have reported using alumina nanoparticles as reinforcing materials in different light alloys processed by several manufacturing processes. For example, Reddy et al. [13] studied the effect of adding alumina nanoparticles in a pure aluminum matrix, combining the use of microwaves, powder metallurgy, and hot extrusion. These results indicated the importance of the dispersion method through powder metallurgy, mainly improving microstructural densification, increment in micro and nano hardness, yield strength, and ultimate strength. The aforementioned is a result of a uniform distribution of the nanoparticles in the aluminum matrix. The obtained results showed that the increase in such properties is proportional to the nanoparticles concentration, up to a maximum volume concentration of 15%. However, other authors reported an increase in the mechanical performance of aluminum alloys manufactured by forging or casting with more modest concentrations (5% by volume), finding an increase in wear resistance and mechanical properties (ultimate tensile strength and yield strength), of 14.3%, 34.3%, and 26.3% respectively, concerning the reference alloy. These results, reported by Al-Salihi et al. [14], were obtained in an A7075 alloy manufactured by stir casting.

On the other hand, Purohit et al. [15] increased the wear resistance in an A356 alloy manufactured by stir and squeeze casting and reinforced with alumina nanoparticles. It is necessary to mention that the results in the wear performance in the alloy modified with nanoparticles, about to the manufacturing method used, indicate that the maximum increase in the mechanical-performance improvement of the modified alloy was reached at a maximum volume of nanoparticles of 3% by volume. The above results indicate that powder metallurgy-based routes allow homogeneous dispersion of alumina nanoparticles in light alloys. Furthermore, the dispersion efficiency of micro and nanoparticles increased by combining processes based on powder metallurgy and mechanical alloying [16].

The mechanical alloying can be used to produce alloys and compounds that are difficult or impossible to obtain by conventional melting as casting techniques [17–20]. The mechanical alloyed technique consists of repeated welding, fracturing, and rewelding of powder particles, leading to particle size variations and changes in the powder particle shape [16]. In this case, under a high-energy impact force, the powder particles are actively deformed. As a result of this energy, strain is introduced in the lattice, and the crystal is fractured into smaller pieces, in this manner promoting the continuous modification of the shape and degree of disorder in the lattice creating defects, such as vacancies, dislocations, stacking faults, and grain boundaries [16,21,22].

The present research involved the synthesis of aluminum composites reinforced with alumina nanoparticles. For this purpose, a combination based on powder metallurgy routes and mechanical alloying was considered. In addition, the wear behavior of the synthesized composites was studied under different load and sliding speed conditions.

2. Materials and Methods

2.1. Synthesis

Table 1 summarizes the chemical composition of the aluminum powders obtained through the machining process of the Al-6061 commercial alloy into metal chips. Here, the reinforcing agent, Al₂O₃ nanoparticles (see Figure 1) had an average size of 20 nm. Composites were produced in a high-energy ball mill Emax. The milling device and milling media used in the experiments were made from hardened steel. The powder mass was 50 g, and 4:1 ball-to-powder weight ratio was prepared. All millings runs were performed with methanol as a process control agent, and Argon as inert milling atmosphere at room temperature. Accordingly, the Al₂O₃ particles concentration was set up to 5 wt.% and the milling time was 5 h. Thus, the compaction of the products was for 2 min under a pressure of 1862.65 MPa. Cold consolidated samples were pressure-less sintered for 3 h at 823 K under vacuum with a 50 K/min heating rate. Sintered products were held at 773 K and hot extruded into a rod of 10 mm in diameter by using indirect extrusion and an extrusion ratio of 16. For comparison purposes, an unreinforced milled, sintered, and hot extruded sample was employed as reference.

Table 1. Chemical composition of the present materials (wt.%).

Aluminums	Al	Cr	Cu	Fe	Mg	Si	Ti	Zn	Al ₂ O ₃
Al-6061	Bal.	0.29	0.18	0.31	1.1	0.15	0.15	0.25	0
Al-6061-Al ₂ O ₃	Bal.	0.29	0.18	0.31	1.1	0.15	0.15	0.25	5

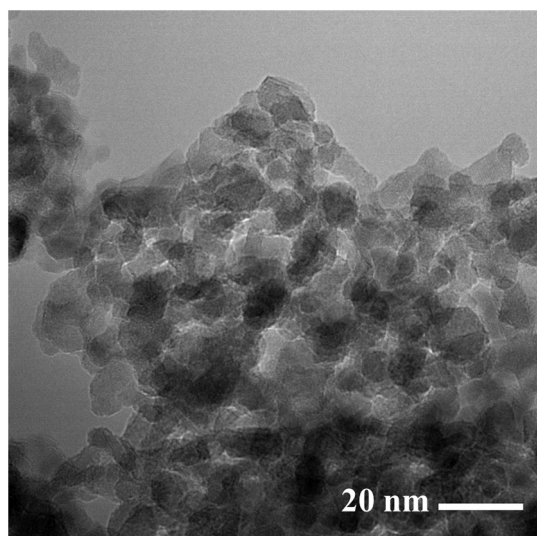


Figure 1. Bright-field TEM micrograph of the Al₂O₃ nanoparticles used as the composites material reinforcement.

2.2. Experimental Characterization

The tribometer (ball-on-disc configuration) used in this research work was Anton Paar TRB[®] (Anton Paar Mexico S. A. de C. V., Hidalgo, Mexico). The aluminum alloy (Al-6061) and the composite (Al-6061-Al₂O₃) were worn for 188.5 m against a 6 mm diameter counterface made of Sapphire (9 on the Mohs scale). Wear tests were carried out at room temperature (~25 °C) at three different levels of load (1, 2, 3 N) and sliding speed (4, 7, 10 cm/s). In previous wear tests, all specimens were polished until a 1-micron diamond paste was produced. At least two samples for each condition were tested, according to ASTM G99-17 [23].

Microhardness Vickers tests were carried out with a load of 100 g (HV/100) applied during 10 s according to ASTM E 384-17 [24], with a hardness tester Tukon 2500[™] (Illinois

Tool Works Inc., Glenview, IL, USA). The average wear rate was calculated with the wear track profile, which was measured with a profilometer Taylor Hobson® (Taylor Hobson Inc., Queretaro, Mexico), and the friction coefficient was measured during each test by the relation between the load sensed by the tribometer and the applied load. Scanning electron microscopy (SEM) and energy dispersive spectroscopy (EDS) were employed to analyze worn surfaces on the samples and collected debris. Wear debris was characterized by X-ray diffraction (XRD) using $K\alpha$ -Cu radiation (45 kV-40 mA) in an interval of 2θ from 20° to 85° with a scanning step size of 0.013° and counting time of 13.77 s.

3. Results

3.1. Characterization of Aluminum Matrix Composites

3.1.1. Distribution of Al_2O_3 Nanoparticles

As can be seen from Figure 2a, a homogeneous distribution of Al_2O_3 nanoparticles is shown, with their agglomeration in colonies homogeneously dispersed along with the aluminum matrix, with an average size of approximately 0.5 to 1 μm in spherical-shape particles bunches. Additionally, Figure 2b presents the SEM-EDS as of one of the agglomerated nanoparticles, wherein it is possible to detect high oxygen content that is one of the main elements that constitute the Al_2O_3 reinforcement. On the other hand, Figure 2c shows some agglomerated nanoparticles, where an oxygen content reduction can be seen due to the majority concentration of the matrix. In this context, Zaiemyekheh et al. [25] suggested that the homogeneous distribution of Al_2O_3 nanoparticles in an aluminum matrix composite reveals the correct use of the process to fabricate the specimens.

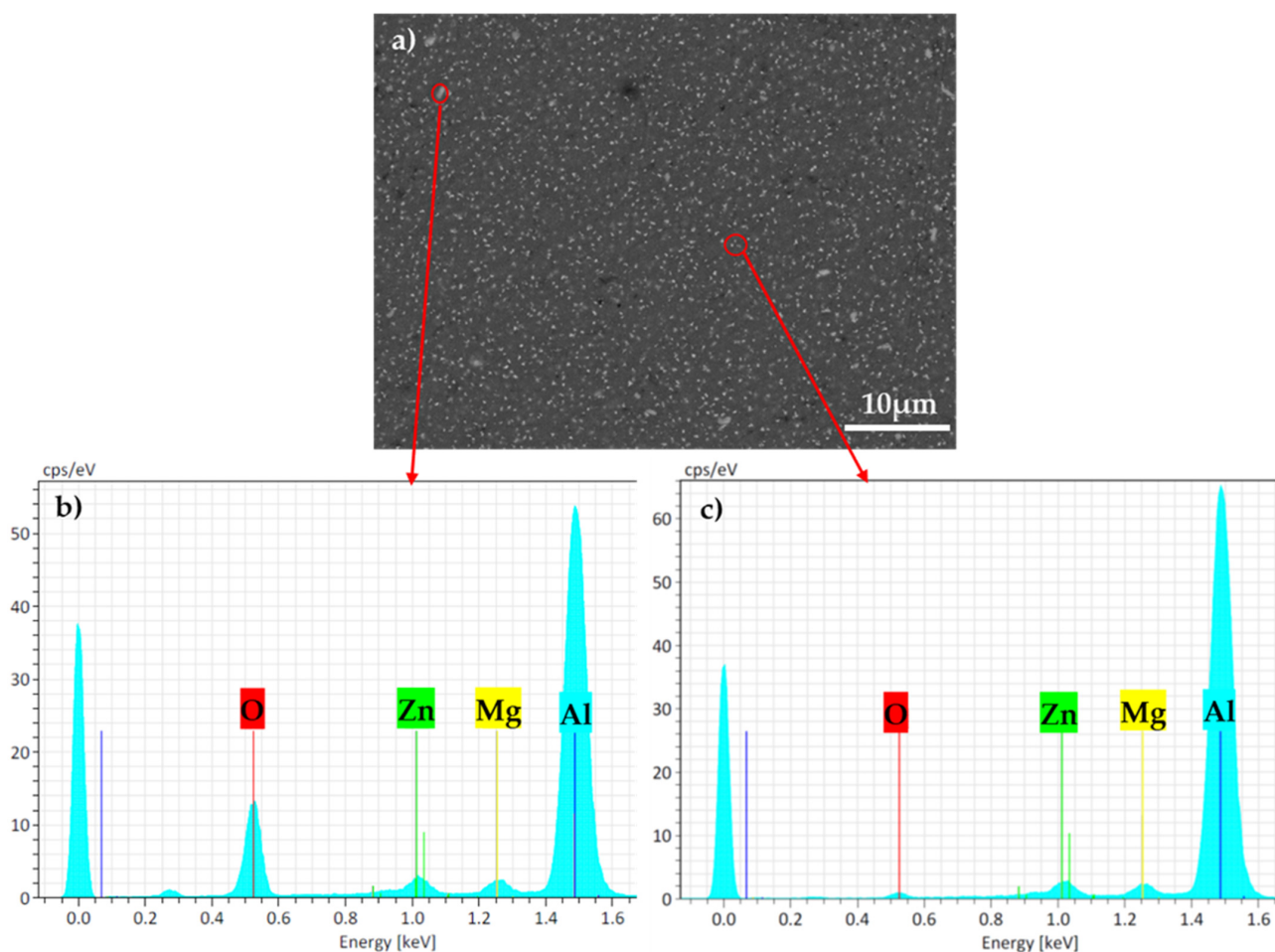


Figure 2. SEM micrographs of the Al_2O_3 nanoparticles distribution in the aluminum matrix composite, (a) $5000\times$, (b) SEM-EDS analysis of one agglomerated nanoparticles, and (c) SEM-EDS analysis of some agglomerated nanoparticles.

3.1.2. Microhardness Vickers Results

Figure 3 shows microhardness results for both materials (Al-6061 and Al-6061-Al₂O₃ with 5 wt.% nanoparticles) and their respective Vickers indent footprints (see Figure 4), in the last figures, it is possible to observe a reduction in the indent footprint of the Al-6061-Al₂O₃ in comparison with the Al-6061, due to the high mechanical resistance obtained by nanoparticles, as will be seen later.

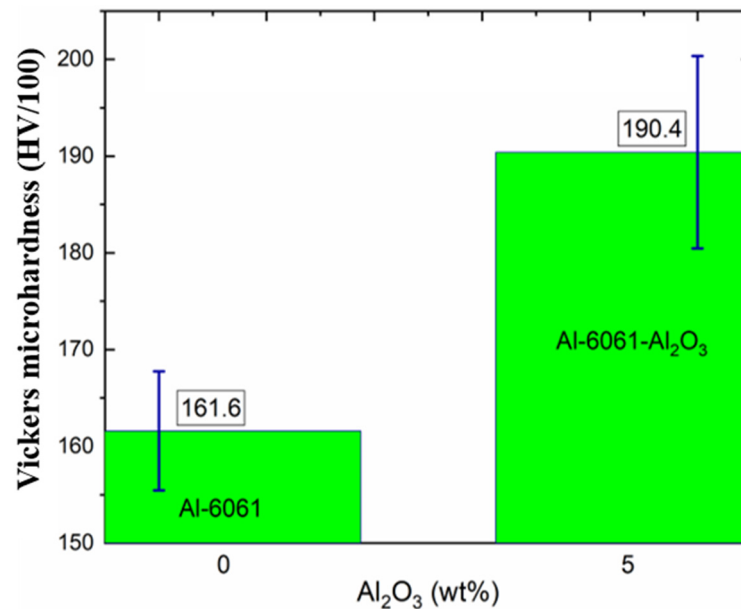


Figure 3. Microhardness results for 0% and 5% of Al₂O₃ nanoparticles in the Al-6061.

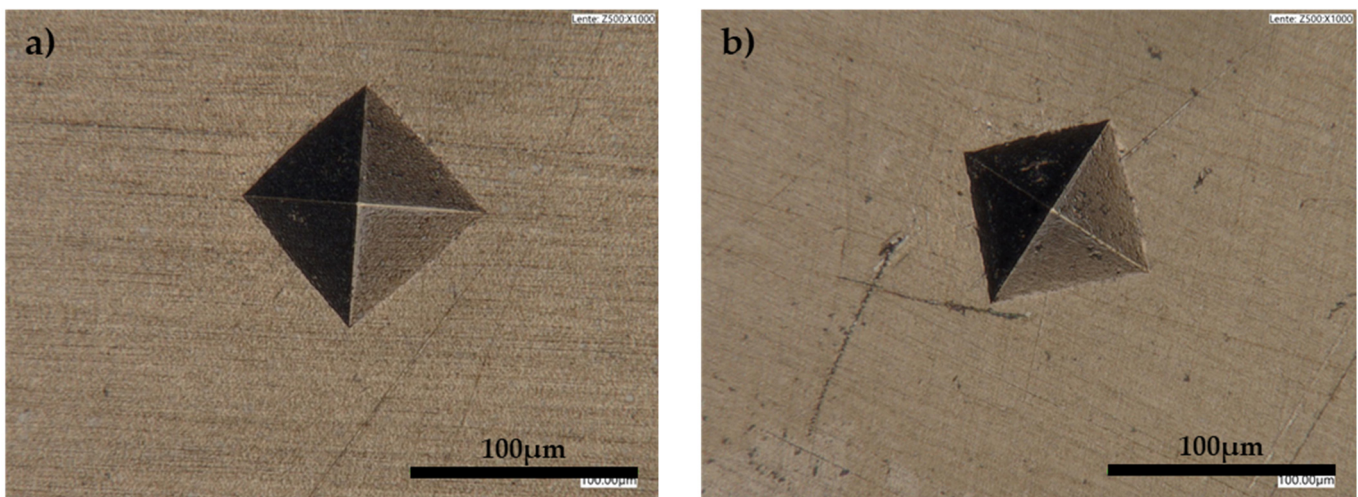


Figure 4. Vickers indent footprint, (a) Al-6061 and (b) Al-6061-Al₂O₃.

Results presented in Figure 3 show that microhardness was significantly higher in the Al-6061-Al₂O₃ than in the Al-6061 alloy. In this part, several strengthening mechanisms are considered, such as thermal mismatch during the sintering stage. However, due to the nature of the synthesis process, an important strengthening mechanism considers the excellent dispersion of the nanoparticles during the milling process [26,27], producing an efficient transfer load from the matrix to the reinforcement. Furthermore, due to the size of the reinforcement, the dispersion of these fine nanometric ceramic particles in the alloy produces free path obstacles in the movement of dislocations in the subgrain structure, enhancing their hardness [28]. Additionally, hard particles of Al₂O₃ can be associated with

stress concentration around particle corners which tends to be reduced as a function of the reduction in the size of alumina particles, as was suggested by Mamoon [29]. In their studies about the effect of different sizes of Al₂O₃ nanoparticles on 6066AA and 7005AA composites on mechanical properties, it was mentioned that 20 nm particle size enhances the best mechanical properties like UTS (Ultimate Tensile Stress). In this context, it is essential to note that the same size was used in the present work.

On the other hand, the nanoparticles concentration considered in this study (5 wt.%) produced a noticeable increase in the mechanical performance evaluated by hardness, significantly increasing the compressive strength. In this regard, Corrochano et al. [30] suggested that smaller reinforcement particles into aluminum matrix composites via powder metallurgy enhance their wear performance as a function of the hardness behavior.

In contrast, Ghasem et al. [31] showed that up to 3 h milled time, as was used in the present research work, promotes the excellent dispersion of fine particles of Al₂O₃ into the aluminum matrix that contributes to increased mechanical properties. It is well known that fine nanoparticles increase dislocation density around the reinforcing particles, and simultaneously, grain refinement occurs due to particle stimulate nucleation mechanisms.

Likewise, Ramezanalizadeh [32] suggested that due to long milled time, reinforcing particles can be trapped into the metal matrix, promoting an increase in the local deformation and promoting the particle welding process, enhancing their final mechanical properties.

3.2. Wear Test Results

3.2.1. Average Wear Rate

Figure 5 shows the average wear rate of the specimens as a function of the applied load for the alloy and the composite (Al-6061 and Al-6061-Al₂O₃ with 5 wt.% nanoparticles, respectively). Again, a similar trend in the wear behavior in both materials was observed: the average wear rate increased as load and sliding speed increased. In this regard, it was suggested that an increment in the applied load tends to increase the penetration of hard asperities of the counterface into the softer sample under evaluation, which generates the removal of particles in the softer material [33–37].

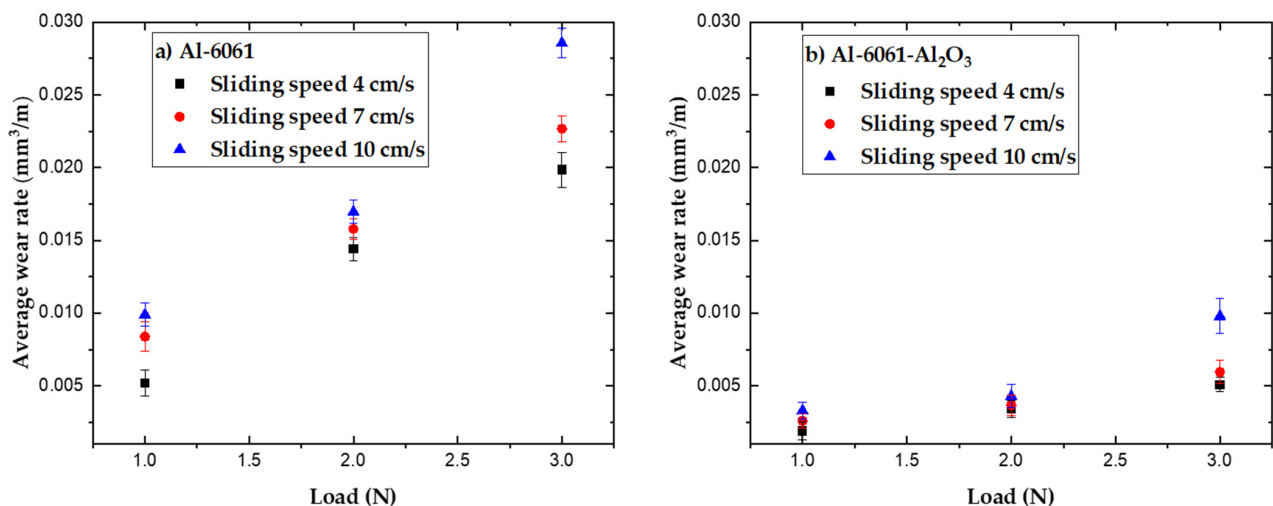


Figure 5. Average wear rate vs. load. (a) Al-6061 and (b) Al-6061-Al₂O₃.

The Al-6061-Al₂O₃ significantly enhances the wear resistance of the composite in comparison with the reference alloy due to the nanoparticles acting as a third hard body that tends to reduce the counterface penetration. Similar trends were found by Sozhamannan et al. [37] in their studies about the wear performance of 6061 Al/nano ticp/Gr hybrid composites, where it was suggested that the presence of reinforcements in the Al matrix restrict the plastic deformation in the initial stage of loading, allowing a subsequent plastic

deformation mildly. In addition, it is important to mention that there exist three important parameters that promote the current wear behavior: friction, temperature, and third body interaction. The researchers suggest that friction between contact surfaces promotes an increment in the temperature that stimulates oxide formations. This oxide formation can act as a solid lubricant that tends to reduce the friction coefficient. Therefore, its stability can be related to the specific conditions of load and sliding speed. Finally, additional reinforced particles well attached to the substrate can improve their mechanical properties as a function of their hardness increment. Parameters such as friction coefficient, oxide formations, and nanoparticle interaction will be discussed in other sections.

3.2.2. Friction Coefficient

Figures 6 and 7 show friction coefficients as a function of the applied load and sliding speed for both materials (Al-6061 and Al-6061-Al₂O₃).

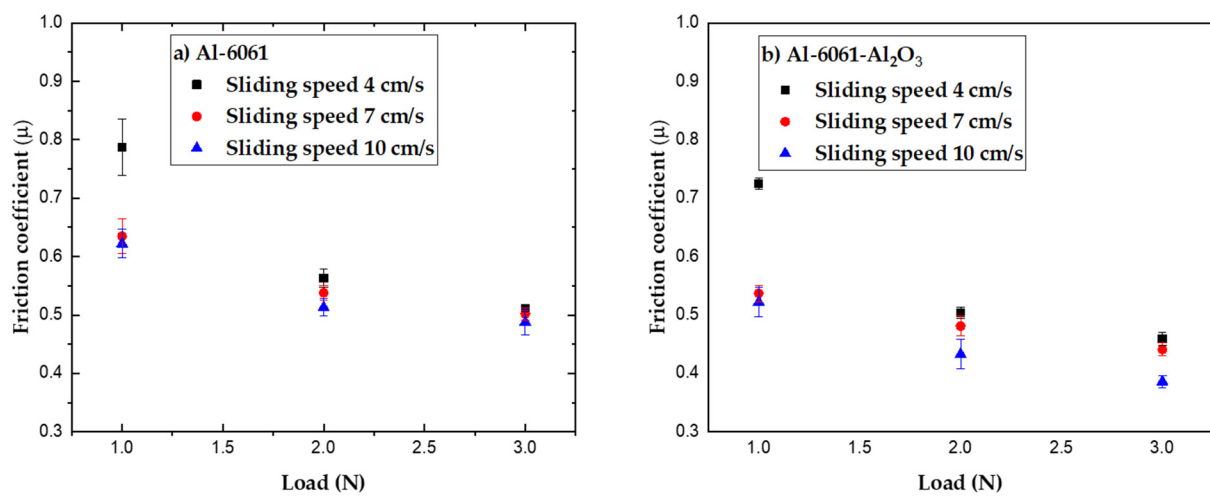


Figure 6. Friction coefficient vs. load. (a) Al-6061 and (b) Al-6061-Al₂O₃.

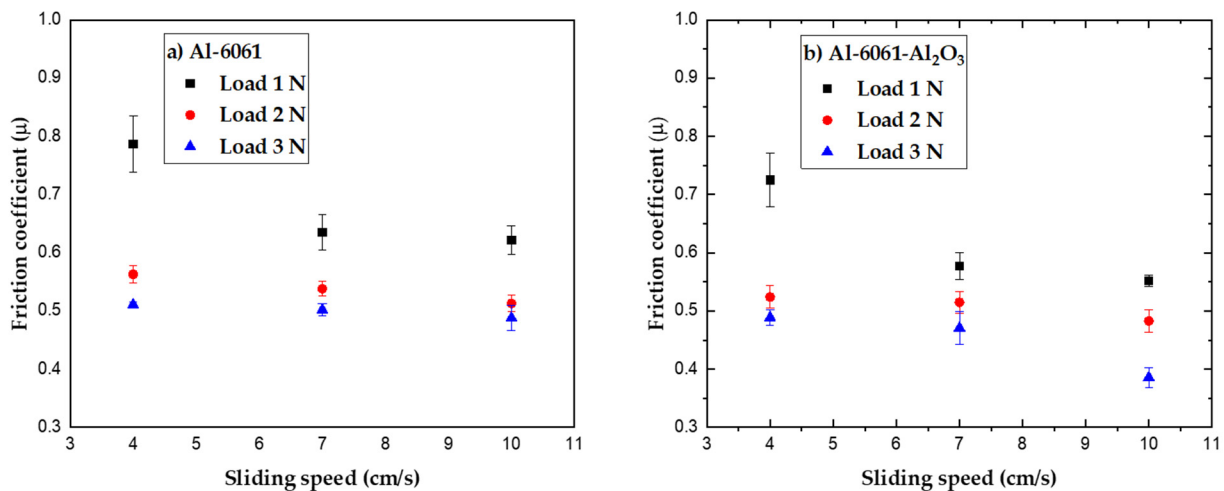


Figure 7. Friction coefficient vs. sliding speed. (a) Al-6061 and (b) Al-6061-Al₂O₃.

The friction coefficient, depicted in Figures 6 and 7, decreases as load and sliding speed increases, which suggests the presence of a fine oxide layer well attaches to contact surfaces mainly at higher loads and speeds, acting as a solid lubricant and reducing the friction coefficient. On the other hand, the Al-6061 with 5 wt.% nanoparticles of alumina (Al₂O₃) reduces the friction coefficient compared with the unreinforced alloy. Hence, the ceramic particles of alumina (Al₂O₃) on a composite material minimize the real contact

area between asperities of samples under evaluation and counterface, reducing the friction coefficient, according to Sardar et al. [38].

3.3. XRD Analysis of Wear Debris and Base Material

Figure 8a,b show XRD patterns of wear debris for both materials (Al-6061 and Al-6061- Al_2O_3 with 5 wt.% nanoparticles) for four test conditions: 1 N and 4 cm/s (low conditions of load and sliding speed), 2 N and 7 cm/s (medium conditions of load and sliding speed), 2 N and 10 cm/s (medium conditions of load and high sliding speed), and 3 N and 10 cm/s (high conditions of load and sliding speed).

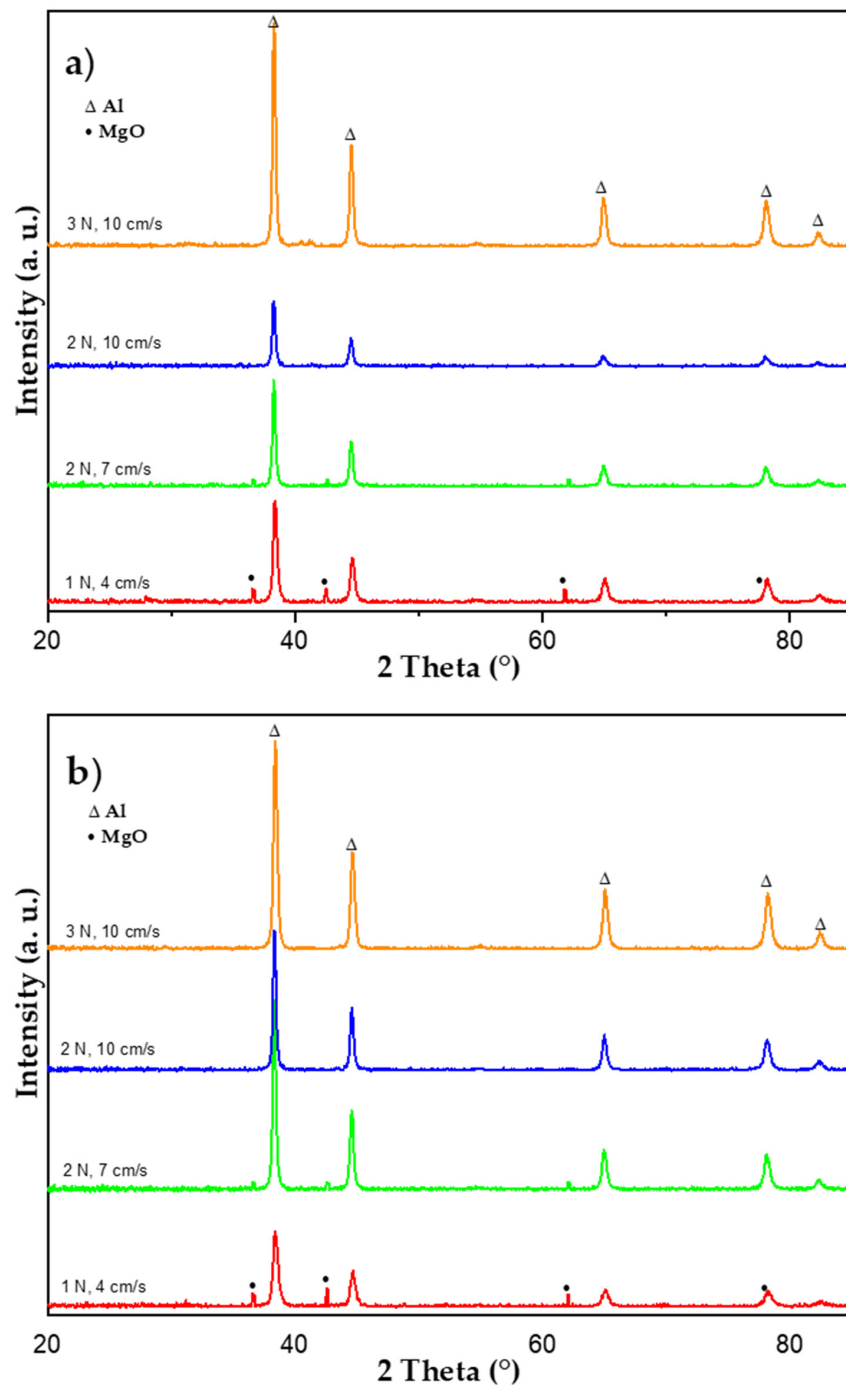


Figure 8. XRD patterns of wear debris, (a) Al-6061 and (b) Al-6061- Al_2O_3 .

According to the XRD results, wear mechanisms observed in the aluminum composite indicate that removing fragments of the matrix is possible because of the material transferred to the counterface by adhesion [39]. The continuous cyclic loading tends to form harden asperities on the counterface (in this case, the sapphire ball), removing material from a sample made of aluminum (alloy and composite).

The detection of a second phase identified as MgO product of the high temperatures reached during the different test conditions can be observed in the XRD patterns. This phase is related to the formation of a tribolayer that reduces the friction coefficient, but cannot be well attached to substrate in order to reduce the wear rate [40]. This oxide formation seems to disappear as load and sliding speed increases. In a range from low load and sliding speed (1 N, 4 cm/s) to medium load and sliding speed (2 N, 7 cm/s), the MgO formation is evident, but in a range from medium load and high sliding speed (2 N, 10 cm/s) to high load and sliding speed (3 N, 10 cm/s), the MgO formation was not detected. This behavior suggests that under low and medium load and sliding speed (1 N, 4 cm/s to 2 N, 7 cm/s), more oxide formations are detached from the contact surface in comparison with a range from 2 N, 10 cm/s to 3 N, 10 cm/s.

It is essential to mention that only with oxygen atmosphere contact [41], the reaction: $2\text{Mg} + \text{O}_2 \rightarrow 2\text{MgO}$ is promoted, and in this case intensified by the dry sliding conditions. In this context, it is evident that the oxide formation is another important parameter to be considered, as not all conditions showing the MgO formation or is not possible to be detected due to the low amount. Therefore, it is suggested that the oxide formation is related to the specific conditions of load and sliding speed that sometimes can act favorable (acting as solid lubricant) and other times unfavorable (acting as abrasive particles). In the same way, Cheng et al. [42] reported in their studies about the evolution of surface oxide film of typical aluminum alloys such as: 1060, 3003, 4032, 5052, 5083, and 6061, that MgO is one of the main stoichiometries formed in aluminum alloys, which is in good agreement with the obtained results.

3.4. SEM Analysis of Worn Surfaces

3.4.1. Worn Surfaces Analysis

Figures 9 and 10 show backscatter secondary electron (BSE) micrographs of worn surfaces with their respective analysis EDS (energy-dispersive X-ray spectroscopy), under conditions of 1 N and 4 cm/s (low conditions of load and sliding speed), 2 N and 7 cm/s (medium conditions of load and sliding speed), and 3 N and 10 cm/s (high conditions of load and sliding speed) for both materials (Al-6061 and Al-6061-Al₂O₃ with 5 wt.% nanoparticles).

From Figures 9a–c and 10a–c, two main zones can be observed. The first one corresponds to a white zone identified as the base material, which is supported by the SEM-EDS analysis (Figures 9a–c and 10a–c (1)), where the low content of oxygen and several of the elements that constitute the aluminum matrix composite (Al, Zn, Mg, Cu) can be detected. In addition, a second dark zone depicts a mixture of delamination and fragmentation of a fine oxide layer; the morphology suggests particles of the counterface. Again, the SEM-EDS analysis supports the evidence (Figures 9a–c and 10a–c (2)) where it is possible to observe high oxygen content. It is evident that a change in tonality from white (base material) to dark (mixture of delamination and compaction of the suggested fine oxide layer) occurs as load and sliding speed increases, which reduces the friction coefficient, but cannot be sufficient to reduce the wear rate. This behavior is in concordance with the XRD results, wherein it was possible to detect MgO in the wear debris, mainly at low and medium load and sliding speed, which suggests high degradation of the fine oxide layer.

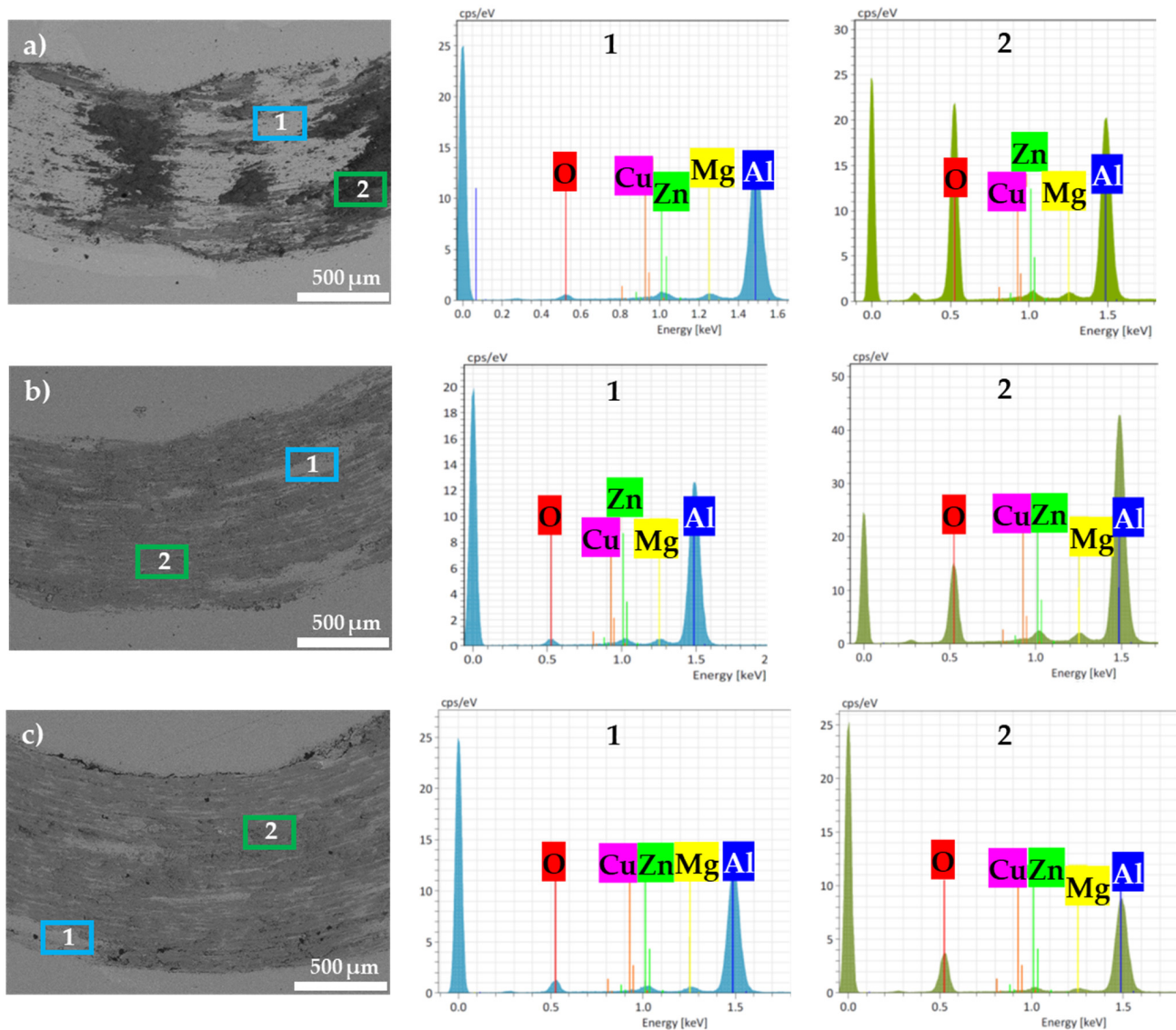


Figure 9. SEM micrographs: backscatter secondary electrons (BSE) and two areas analyzed with SEM-EDS of the Al-6061 aluminum alloy, under low, medium, and high conditions of load and sliding speed ((a) 1 N and 4 cm/s, (b) 2 N and 7 cm/s, (c) 3 N and 10 cm/s).

Additionally, the width of wear tracks increased as load and sliding speeds increased (see Figures 9a–c and 10a–c). These results are related to the increment in the penetration of the counterface as load and sliding speed increase. On the other hand, a diminution of the wear track thickness in the Al-6061- Al_2O_3 with 5 wt.% nanoparticles was also observed (Figure 10a–c) in comparison with the Al-6061 without nanoparticles (Figure 9a–c), which suggests a protective behavior of the nanoparticles (Al_2O_3) in the aluminum matrix composites.

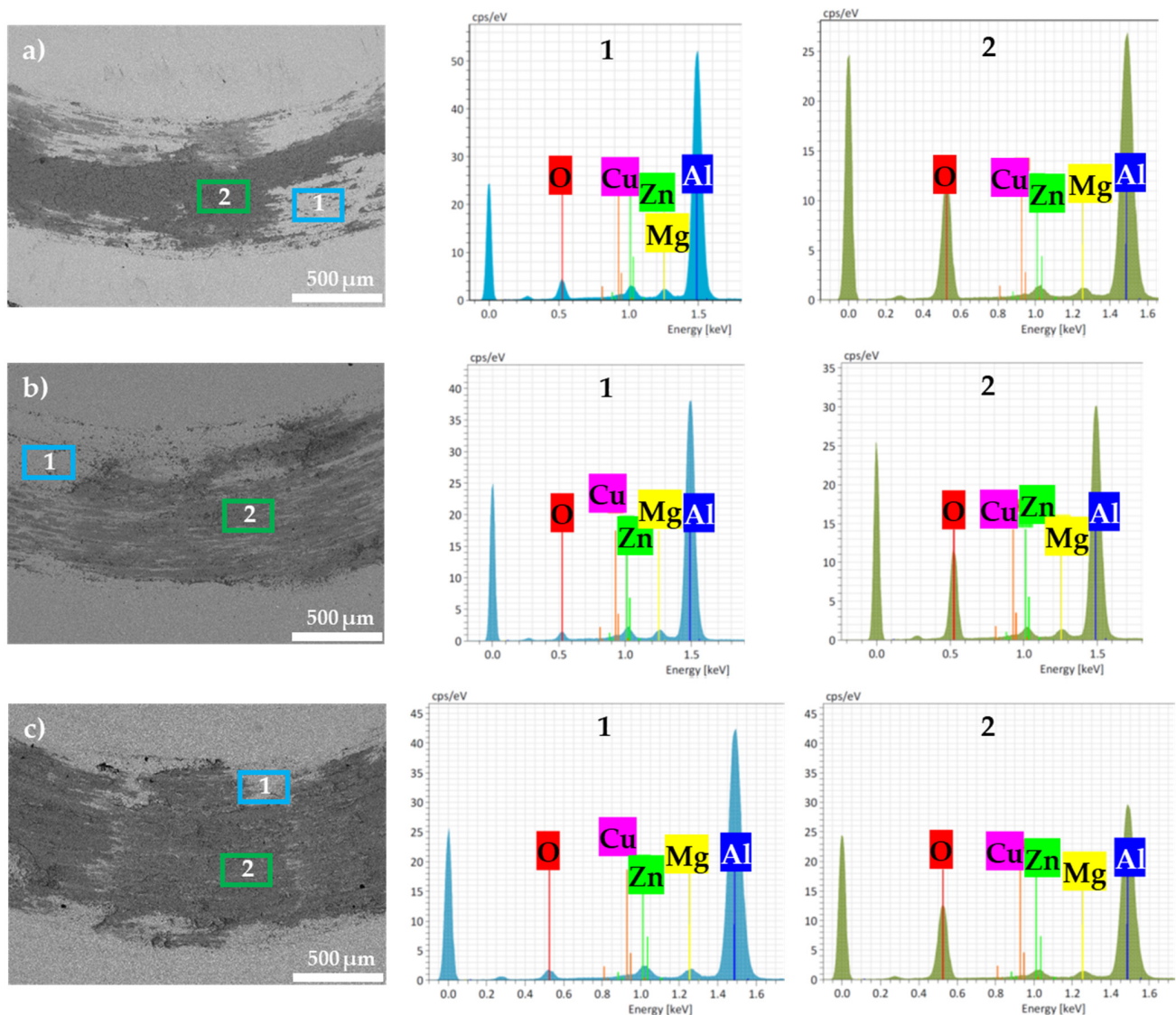


Figure 10. SEM micrographs: backscatter secondary electrons (BSE) and two areas analyzed with SEM-EDS of the Al-6061- Al_2O_3 aluminum composite, under low, medium, and high conditions of load and sliding speed ((a) 1 N and 4 cm/s, (b) 2 N and 7 cm/s, (c) 3 N and 10 cm/s).

3.4.2. Surface and Elemental Mapping Analysis

Figure 11 displays SEM images of the worn surfaces at high magnification ($2000\times$) and elemental mappings via EDS under conditions of low load and sliding speed (1 N, 4 cm/s), medium load and sliding speed (2 N, 7 cm/s), and high load and sliding speed (3 N, 10 cm/s) for both materials (Al-6061 and Al-6061- Al_2O_3 with 5 wt.% nanoparticles).

Wear debris composed of the suggested fine oxide layer and the base material can be observed. A reduction in the fine oxide wear particles was detected as the load and sliding speed increased, which suggests a transition from oxidative to adhesive behavior, related to an initial high content of oxide wear debris and a long shallow crater surface. A wear map developed by Raghavendra and Ramamurthy [43] showed that in the Al 7075 reinforced with 5 wt.% of Al_2O_3 , a transition of mild wear (oxidation) to severe wear (large crater and grooves) can occur as load and sliding speed increases. These observations are according to the presented results, the same behavior is shown in both materials (Al-6061 and Al-6061- Al_2O_3 with 5 wt.% nanoparticles). Furthermore, it is observed that there is delamination and compaction of the suggested tribo-layer formed under the current

conditions, a product of the different conditions of load, sliding speed, and the rotary ball-on-disc conditions.

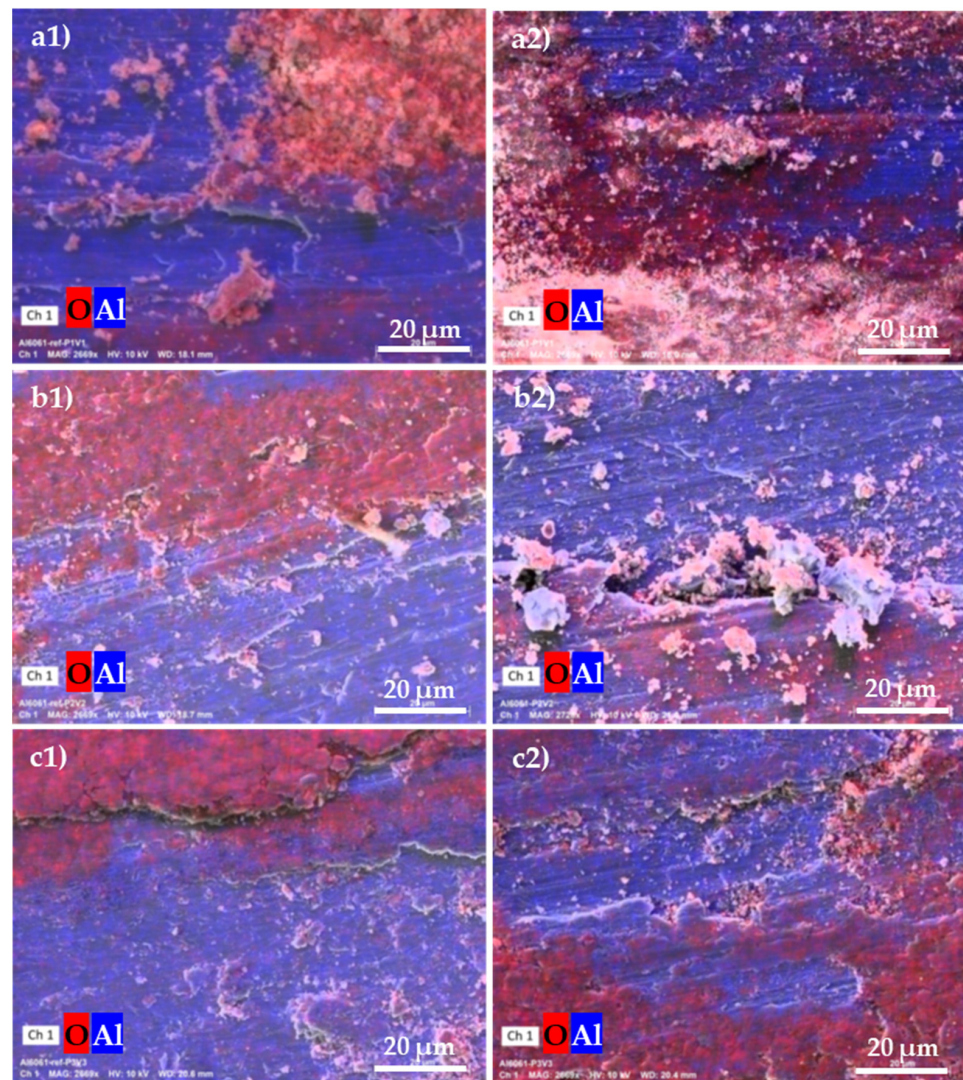


Figure 11. Elemental mapping of worn surface at high magnification for the Al-6061 aluminum alloy (a1–c1) and aluminum composite (a2–c2), under low, medium, and high conditions of load and sliding speed (1 N and 4 cm/s, 2 N and 7 cm/s, 3 N and 10 cm/s).

Differences are present on contact surfaces, mainly with fine oxide wear particles. In this context, it is possible to corroborate the high presence of fine oxide wear particles, whose content tends to be more pronounced at low and medium load and sliding speed (1 N and 4 cm/s) (2 N and 7 cm/s). Thus, the latest suggests the presence of a fine oxide film that reduces the friction coefficient, but it is not sufficient to generate wear protection. In the opposite way, at high load and sliding speed (3 N and 10 cm/s), the presence of oxide wear particles on worn surfaces was not detected, which is related to the low degradation of the suggested fine oxide layer. These results are in concordance with the XRD patterns applied on wear debris, where it is possible to detect oxide formations at low and medium load and sliding speed (1 N and 4 cm/s) (2 N and 7 cm/s), due to the high degradation of the suggested fine oxide layer. On the other hand, at high load and sliding speed (3 N and 10 cm/s), it was not possible to detect oxide formations, due to the low degradation of the suggested fine oxide layer.

3.4.3. Nanoparticle Analysis in the Wear Fragments

SEM images of the wear fragments after wear tests in the Al-6061-Al₂O₃ with 5 wt.% nanoparticles show the distribution of alumina nanoparticles in the wear fragments (see Figure 12). Here, it is possible to observe that Al₂O₃ particles appear embedded into the aluminum matrix composite. In this context, the literature suggests that the separation of abrasive particles such as oxides, carbides, nitrides, and others from the metal matrix can accelerate the removal of particles during wear tests which, as seen in this work, does not happen [34,35,38,39,44]. Particles embedded into the metal matrix can help enhance their wear performance due to an effective load transfer from the matrix to the reinforcement, as shown in the present study.

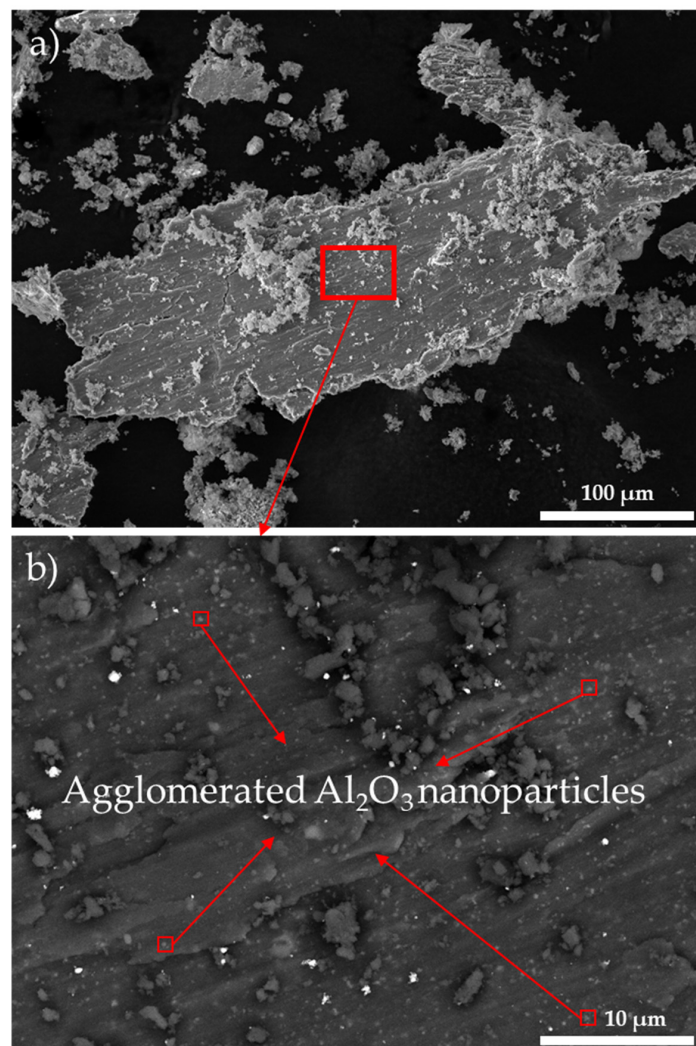


Figure 12. SEM micrographs of Al₂O₃ nanoparticles in the wear fragments. (a) 600× and (b) 6000×.

3.4.4. Schematic Illustration of the Wear Performance

Due to the depicted evidence, it is possible to suggest the next schematic wear evolution with the conditions presented:

Figures 13 and 14 show that both materials (Al-6061 and Al-6061-Al₂O₃ with 5 wt.% nanoparticles) form an oxide layer (MgO), which tends to reduce the direct contact between counterface and base material, showing the presence of fine and agglomerate particles coated with high oxygen content, as it was stated above. In this context, a reduction in the friction coefficient was evident as load and sliding speed increased, but not sufficient to generate wear protection. The wear protection is attained to the increment in hardness.

On the other hand, it is evident that degradation of fine wear particles at the initial stage of load and sliding speed occurs, which tend to be less pronounced as load and sliding speed increased. In this regard, it is important to mention that the addition of alumina nanoparticles significantly increases the wear resistance of the composites in comparison with the alloy, as a function of their hardness [25,45].

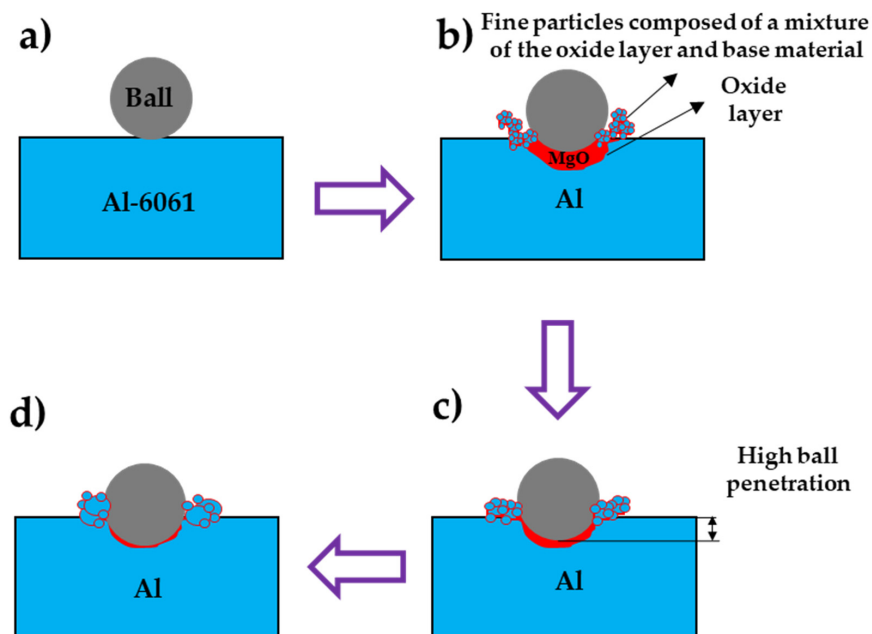


Figure 13. Schematic representation of wear evolution in the Al-6061 aluminum alloy. (a) Initial conditions, (b) first evolution of wear test, (c) second evolution of wear test, and (d) final evolution of wear test.

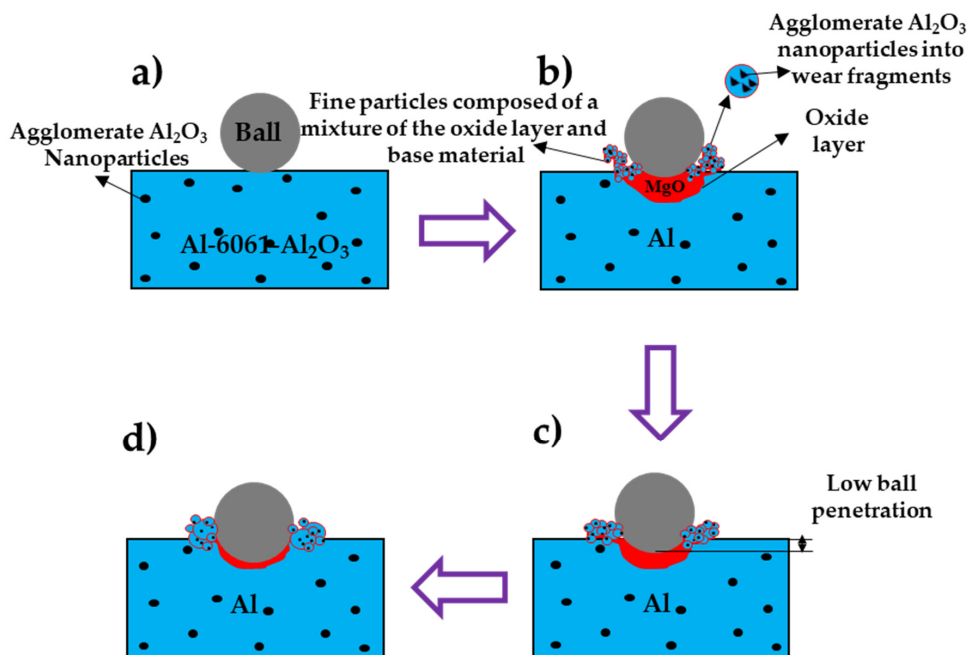


Figure 14. Schematic representation of wear evolution in the Al-6061-Al₂O₃ aluminum composite. (a) Initial conditions, (b) first evolution of wear test, (c) second evolution of wear test, and (d) final evolution of wear test.

4. Conclusions

The analysis performed on the experimental results showed a significant improvement on the average wear rate of the aluminum matrix composite with 5 wt.% nanoparticles (Al-6061-Al₂O₃) compared with the aluminum base alloy without nanoparticles (Al-6061). This improvement in the wear rate is attributable to the hard nanoparticles of alumina (Al₂O₃) that act as a third hard body against wear, reducing the penetration of the counterface into the softer materials. Furthermore, the mechanical properties of the aluminum matrix composites were improved due to the addition of alumina (Al₂O₃) nanoparticles. Strengthening mechanisms mainly lie in a nanometric size and homogeneous dispersion of particles offering an effective load transfer from the matrix to the reinforcement.

XRD results show the formation of a fine oxide (MgO) that tends to reduce the friction coefficient as load and sliding speed increases, due to acting as a solid lubricant. This oxide formation was especially detected on wear debris at low and medium load (1, 2 N) and low and medium sliding speed (4, 7 cm/s), where it was easier to detect this behavior, which is related to the high degradation of the suggested oxide film in these conditions. On the other hand, the oxide formation tended to disappear at high load and sliding speed (3 N and 10 cm/s), which suggests low degradation of the oxide film in this other condition.

SEM results showed fine oxide wear fragments on the contact surface, especially at low and medium load and sliding speed (1 N and 4 cm/s) (2 N and 7 cm/s), a product of the degradation of the suggested tribo-film, where this fine oxide wear fragments appeared to disappear as load and sliding speed increased. Finally, it was evident that alumina nanoparticles (Al₂O₃) were maintaining embedded into wear fragments after wear tests, offering excellent wear properties.

Author Contributions: Conceptualization, V.H.M.-L.; data curation, H.A.-G., M.H.-H. and I.E.G.; formal analysis, V.H.M.-L., M.H.-H., I.E.G. and J.A.B.-C.; funding acquisition, V.H.M.-L.; investigation, V.H.M.-L., J.C.D.-G., H.A.-G. and R.P.-B.; methodology, V.H.M.-L., C.D.G.-E., J.C.D.-G. and R.P.-B.; project administration, V.H.M.-L.; resources, C.D.G.-E., I.E.G. and J.A.B.-C.; software, H.A.-G.; supervision, J.C.D.-G. and R.P.-B.; validation, V.H.M.-L., J.M.-C., A.G.-M. and H.A.-G.; visualization, C.D.G.-E. and H.A.-G.; writing—original draft, V.H.M.-L.; writing—review and editing, V.H.M.-L., J.C.D.-G., J.M.-C., A.G.-M., J.A.B.-C. and R.P.-B. All authors have read and agreed to the published version of the manuscript.

Funding: This research received no external funding.

Institutional Review Board Statement: Not applicable.

Informed Consent Statement: Not applicable.

Data Availability Statement: All data are available if they are required, request to the corresponding authors.

Acknowledgments: Authors would like to thank the National Council on Science and Technology (CONACYT-México) for the support through the Cátedras CONACYT program by project grant number 850, 674, FMSLP-2019-01-01-215684, and CB-257705.

Conflicts of Interest: The authors declare no conflict of interest.

References

1. Zhao, C.; Zhou, J.; Mei, Q.; Ren, F. Microstructure and dry sliding wear behavior of ultrafine-grained Co-30 at% Cr alloy at room and elevated temperatures. *J. Alloys Compd.* **2019**, *770*, 276–284. [[CrossRef](#)]
2. Khamis, S.S.; Lajis, M.A.; Albert, R.A.O. A sustainable direct recycling of aluminum chip (AA6061) in hot press forging employing response surface methodology. *Procedia CIRP* **2015**, *26*, 477–481. [[CrossRef](#)]
3. Chen, C.-L.; Lin, C.-H. In-situ dispersed La oxides of Al6061 composites by mechanical alloying. *J. Alloys Compd.* **2019**, *775*, 1156–1163. [[CrossRef](#)]
4. Kuforiji, C.; Nganbe, M. Powder metallurgy fabrication, characterisation and wear assessment of SS316L-Al₂O₃ composites. *Tribol. Int.* **2019**, *130*, 339–351. [[CrossRef](#)]
5. Shaikh, M.B.N.; Arif, S.; Azis, T.; Waseem, A.; Shaikh, M.A.N.; Ali, M. Microstructural, mechanical and tribological behaviour of powder metallurgy processed SiC and RHA reinforced Al-based composites. *Surf. Interfaces* **2019**, *15*, 166–179. [[CrossRef](#)]

6. Park, K.; Park, J.; Kwon, H. Effect of intermetallic compound on the Al-Mg composite materials fabricated by mechanical ball milling and spark plasma sintering. *J. Alloys Compd.* **2018**, *739*, 311–318. [[CrossRef](#)]
7. Sohi, M.H.; Hojjatzadeh, S.M.H.; Moosavifar, S.S.; Heshmati-Manesh, S. Liquid phase surface melting of AA8011 aluminum alloy by addition of Al/Al₂O₃ nano-composite powders synthesized by high-energy milling. *Appl. Surf. Sci.* **2014**, *313*, 76–84. [[CrossRef](#)]
8. Krishnan, P.K.; Christy, J.V.; Arunachalam, R.; Mourad, A.-H.I.; Muraliraja, R.; Al-Maharbi, M.; Murali, V.; Chandra, M.M. Production of aluminum alloy-based metal matrix composites using scrap aluminum alloy and waste materials: Influence on microstructure and mechanical properties. *J. Alloys Compd.* **2019**, *784*, 1047–1061. [[CrossRef](#)]
9. Balaraj, V.; Kori, N.; Nagaral, M.; Auradi, V. Microstructural evolution and mechanical characterization of micro Al₂O₃ particles reinforced Al6061 alloy metal composites. *Mater. Today Proc.* **2021**, *47*, 5959–5965. [[CrossRef](#)]
10. Veeresh Kumar, G.B.; Pramod, R.; Rao, C.S.P.; Gouda, P.S.S. Artificial neural network prediction on wear of Al6061 alloy metal matrix composites reinforced with -Al₂O₃. *Mater. Today Proc.* **2018**, *5 Pt 2*, 11268–11276. [[CrossRef](#)]
11. Akbar, H.I.; Surojo, E.; Ariawan, D.; Prabowo, A.R. Experimental study of quenching agents on Al6061–Al₂O₃ composite: Effects of quenching treatment to microstructure and hardness characteristics. *Results Eng.* **2020**, *6*, 100105. [[CrossRef](#)]
12. Pournaderi, S.; Akhlaghi, F. Wear behaviour of Al6061-Al₂O₃ composites produced by in-situ powder metallurgy (IPM). *Powder Technol.* **2017**, *313*, 184–190. [[CrossRef](#)]
13. Reddy, M.P.; Ubaid, F.; Shakoor, R.A.; Parande, G.; Manakari, V.; Mohamed, A.M.A.; Gupta, M. Effect of reinforcement concentration on the properties of hot extruded Al-Al₂O₃ composites synthesized through microwave sintering process. *Mater. Sci. Eng. A* **2017**, *696*, 60–69. [[CrossRef](#)]
14. Al-Salihi, H.A.; Mahmood, A.A.; Alalkawi, H.J. Mechanical and wear behavior of AA7075 aluminum matrix composites reinforced by Al₂O₃ nanoparticles. *Nanocomposites* **2019**, *5*, 67–73. [[CrossRef](#)]
15. Purohit, R.; Qureshi, M.M.U.; Jain, A. Forming behaviour of aluminium matrix nano Al₂O₃ composites for automotive applications. *Advances in Materials and Processing Technologies. Adv. Mater. Process. Technol.* **2020**, *6*, 272–283.
16. Suryanarayana, C. Mechanical alloying and milling. *Prog. Mater. Sci.* **2001**, *46*, 1–184. [[CrossRef](#)]
17. Pérez-Bustamante, R.; Pérez-Bustamante, F.; Maldonado-Orozco, M.C.; Martínez-Sánchez, R. The effect of heat treatment on microstructure evolution in artificially aged carbon nanotube/Al2024 composites synthesized by mechanical alloying. *Mater. Charact.* **2017**, *126*, 28–34. [[CrossRef](#)]
18. Mercado-Lemus, V.H.; Pérez-Bustamante, R.; Díaz-Guillén, J.C.; Alvarez-Vera, M.; Arcos-Gutierrez, H.; Mayen, J.; Salas-Reyes, A.E.; Gallegos-Melgar, A.; Hernandez-Hernandez, M.; Acevedo-Davila, J.L. Homogeneous Distribution of Alumina Nanoparticles in the 6061 Aluminum Alloy via Mechanical Alloying. *Microsc. Microanal.* **2020**, *26* (Suppl. S2), 2894–2896. [[CrossRef](#)]
19. Cano-Figueroa, M.A.; Pérez-Bustamante, F.; Pérez-Bustamante, R.; Mercado-Lemus, V.H.; Hernandez-Hernandez, M.; Gomez-Esparza, C.D.; Camarillo-Cisneros, J.; Martínez-Sánchez, R.; Carreño-Gallardo, C.; Mendoza-Duarte, J.M. Microstructural analysis of master alloys processed by mechanical alloying. *Microsc. Microanal.* **2021**, *27* (Suppl. S1), 3390–3392. [[CrossRef](#)]
20. Dayani, D.; Shokuhfar, A.; Vaezi, M.R.; Jafarpour Rezaei, S.R.; Hosseinpour, S. Structural and mechanical evaluation of a nanocrystalline Al-5 wt%Si alloy produced by mechanical alloying. *Metals* **2017**, *7*, 332. [[CrossRef](#)]
21. Betancourt-Cantera, J.A.; Sánchez-De Jesús, F.; Bolarín-Miró, A.M.; Torres-Villaseñor, G.; Betancourt-Cantera, L.G. Magnetic properties and crystal structure of elemental cobalt powder modified by high-energy ball milling. *J. Mater. Res. Technol.* **2019**, *8*, 4995–5003. [[CrossRef](#)]
22. Betancourt-Cantera, L.G.; Sánchez-De Jesús, F.; Bolarín-Miró, A.M.; Gallegos-Melgar, A.; Mayen, J.; Betancourt-Cantera, J.A. Structural analysis and magnetic characterization of ternary alloys (Co-Fe-Ni) synthesized by mechanical alloying. *J. Mater. Res. Technol.* **2020**, *9*, 14969–14978. [[CrossRef](#)]
23. ASTM. Standard Test Method for Wear Testing with a Pin-on-Disk Apparatus. In *ASTM Standard G99-17*; ASTM International: West Conshohocken, PA, USA, 2017. [[CrossRef](#)]
24. ASTM. Standard Test Method for Microindentation Hardness of Materials. In *ASTM Standard E384-17*; ASTM International: West Conshohocken, PA, USA, 2017. [[CrossRef](#)]
25. Zahiemyekheh, Z.; Liaghat, G.H.; Ahmadi, H.; Khan, M.K.; Razmkhah, O. Effect of strain rate on deformation behavior of aluminum matrix composites with Al₂O₃ nanoparticles. *Mat. Sci. Eng. A* **2019**, *753*, 276–284. [[CrossRef](#)]
26. Bhaskar, K.V.; Sundarrajan, S.; Rao, B.S.; Ravindra, K. Effect of reinforcement and wear parameters on dry sliding wear of aluminum composites—A review. *Mater. Today Proc.* **2018**, *5*, 5891–5900. [[CrossRef](#)]
27. Fava, A.; Montanari, R.; Richetta, M.; Testani, C.; Varone, A. Analysis of Strengthening Mechanisms in Nano-ODS Steel Depending on Preparation Route. *J. Mater. Sci. Eng.* **2018**, *7*, 474. [[CrossRef](#)]
28. Aghamiri, S.M.S.; Oono, N.; Ukai, S.; Kasada, R.; Noto, H.; Hishinuda, Y.; Muroga, T. Microstructure and mechanical properties of mechanically alloyed ODS copper alloy for fusion material application. *Nucl. Mater. Energy* **2018**, *15*, 17–22. [[CrossRef](#)]
29. Al-Jaafari, M.A.A. Study the effects of different size of Al₂O₃ nanoparticles on 6066AA and 7005AA composites on mechanical properties. *Mater. Today Proc.* **2021**, *42*, 2909–2913. [[CrossRef](#)]
30. Corrochano, J.; Walker, J.C.; Lieblich, M.; Ibañez, J.; Rainforth, W.M. Dry sliding wear behavior of powder metallurgy Al-Mg-Si alloy MoSi₂ composites and their relationship with the microstructure. *Wear* **2011**, *270*, 658–665. [[CrossRef](#)]
31. Azimi-Roeen, G.; Kashani-Bozorg, S.F.; Nosko, M.; Nagy, S.; Mat'ko, I. Correction to: Formation of Al/(Al₁₃F₄+ Al₂O₃) nano-composites via mechanical alloying and friction stir processing. *J. Mater. Eng. Perform.* **2018**, *27*, 6800. [[CrossRef](#)]

32. Ramezanalizadeh, H. Fabrication and characterization of an Al-based nanocomposite with high specific strength and good elongation using large amount CMA nanoparticles. *J. Alloys Compd.* **2020**, *822*, 153667. [[CrossRef](#)]
33. Annigeri, U.K.; Kumar, G.B.V. Effect of reinforcement on density, hardness and wear behavior of aluminum metal matrix composites: A review. *Mater. Today Proc.* **2018**, *5*, 11233–11237. [[CrossRef](#)]
34. Kumar, M.; Kumaraswamidhas, L.A. Characterization and tribological analysis on 6061 reinforced with AlN and ZrB₂ in situ composites. *J. Mater. Res. Technol.* **2019**, *8*, 969–980. [[CrossRef](#)]
35. Ravindranath, V.M.; Shankar, G.S.S.; Basavarajappa, S.; Kumar, N.G.S. Dry sliding wear behavior of hybrid aluminum metal matrix composite reinforced with boron carbide and graphite particles. *Mater. Today Proc.* **2017**, *4*, 11163–11167. [[CrossRef](#)]
36. Sharma, P.; Khanduja, D.; Sharma, S. Dry sliding wear investigation of Al6082/Gr metal matrix composites by response surface methodology. *J. Mater. Res. Technol.* **2016**, *5*, 29–36. [[CrossRef](#)]
37. Sozhamannan, G.G.; Yusuf, M.M.; Aravind, G.; Kumaresan, G.; Velmurugan, K.; Venkatachalapathy, V.S.K. Effect of applied load on the wear performance of 6061 Al/nano Ticp/Gr hybrid composites. *Mater. Today Proc.* **2018**, *5*, 6489–6496. [[CrossRef](#)]
38. Sardar, S.; Karmakar, S.K.; Das, D. High stress abrasive wear characteristics of Al 7075 alloy and 7075/Al₂O₃ composite. *Measurement* **2018**, *127*, 42–62. [[CrossRef](#)]
39. Pramanik, A. Effects of reinforcement on wear resistance of aluminum matrix composites. *Trans. Nonferr. Met. Soc. China* **2016**, *26*, 348–358. [[CrossRef](#)]
40. Nemati, N.; Emamy, M.; Penkov, O.V.; Kim, J.; Kim, D.-E. Mechanical and high temperature wear properties of extruded Al composite reinforced with Al₁₃Fe₄ CMA nanoparticles. *Mater. Des.* **2016**, *90*, 532–544. [[CrossRef](#)]
41. Housecroft, C.E.; Sharpe, A.G.; Gil Ruiz, P. *Química Inorgánica*, 2nd ed.; Pearson Prentice Hall: Madrid, Spain, 2006; pp. 279–290.
42. Cheng, F.; Zhao, H.; Wang, Y.; Xiao, B.; Yao, J. Evolution of surface oxide film of typical aluminum alloy during medium-temperature brazing process. *Trans. Tianjin Univ.* **2014**, *20*, 54–59. [[CrossRef](#)]
43. Raghavendra, N.; Ramamurthy, V.S. Development and dry sliding wear map for Al 7075/Al₂O₃ particulate composites. *J. Appl. Phys.* **2018**, *5*, 24104–24113. [[CrossRef](#)]
44. Monikandan, V.V.; Joseph, M.A.; Rajendradumar, P.K. Dry sliding wear studies of aluminum matrix hybrid composites. *Resour. Effic. Technol.* **2016**, *2*, S12–S24. [[CrossRef](#)]
45. Archard, J.F. Contact and rubbing on flat surfaces. *J. Appl. Phys.* **1953**, *24*, 981–988. [[CrossRef](#)]